Earth Syst. Dynam. Discuss., 4, 1065–1090, 2013
www.earth-syst-dynam-discuss.net/4/1065/2013/
doi:10.5194/esdd-4-1065-2013

Earth System Dynamics
Discussions
Open Access

Problems with solar, volcanic, and ENSO attribution using multiple linear regression methods on temperatures from 1979–2012

T. Masters

Los Angeles, CA, USA

Received: 8 October 2013 – Accepted: 25 October 2013 – Published: 8 November 2013

Correspondence to: T. Masters (tmasters@ucla.edu)

Published by Copernicus Publications on behalf of the European Geosciences Union.

Abstract

The effectiveness of multiple linear regression approaches in removing solar, volcanic, and El Nino Southern Oscillation (ENSO) influences from the recent (1979–2012) surface temperature record is examined, using simple energy balance and global climate models (GCMs). These multiple regression methods are found to incorrectly diagnose the underlying signal – particularly in the presence of a deceleration – by generally overestimating the solar cooling contribution to an early 21st century pause while underestimating the warming contribution from the Mt. Pinatubo recovery. In fact, one-box models and GCMs suggest that the Pinatubo recovery has contributed more to post-2000 warming trends than the solar minimum has contributed to cooling over the same period. After adjusting the observed surface temperature record based on the natural-only multi-model mean from several CMIP5 GCMs and an empirical ENSO adjustment, a significant deceleration in the surface temperature increase is found, ranging in magnitude from -0.06 to $-0.12\,\mathrm{K\,dec^{-2}}$ depending on model sensitivity and the temperature index used. This likely points to internal decadal variability beyond these solar, volcanic, and ENSO influences.

1 Introduction

Temperature indices suggest a pause or slowdown in the global surface temperature warming at the beginning of the 21st century, despite the continued emission of anthropogenic greenhouse gases into the atmosphere. Various factors have been proposed that may be offsetting the impact of these greenhouse gases, which can be separated into two categories: (a) negative top-of-atmosphere (TOA) forcings, such as decreased solar activity, anthropogenic tropospheric aerosols (Kauffman et al., 2011), volcanic aerosols (Neely et al., 2013), and stratospheric water vapor (Solomon et al., 2010), and (b) internal variability, such as ENSO (Kauffman et al., 2011), the Atlantic Multidecadal Oscillation (Keenlyside et al., 2008), and the Pacific Decadal Oscillation

ESDD
4, 1065–1090, 2013

(Mochizuki et al., 2010), which may have contributed to an increase in the efficiency of ocean heat uptake (Guemas et al., 2013; Watanabe et al., 2013).

In particular, multiple linear regressions have been used to diagnose the impact of what are considered to be among the largest natural contributors to decadal trends – volcanic eruptions, solar irradiance, and ENSO (Lean and Rind, 2008; Foster and Rahmstorf, 2011). The results from Foster and Rahmstorf (2011) suggest that the prolonged solar minimum, in combination with the dominant La Nina phase of ENSO in the early 21st century, are largely sufficient to explain the pause in the global surface temperature increase seen in the various temperature records. That is, once adjusting for these factors using the results of a multiple regression analysis from 1979–2010, there is no indication of such a slowdown.

In this study, we investigate the effectiveness of this multiple linear regression method – using volcanic, solar, and ENSO indices and a linear time trend in the regressions – in diagnosing the underlying warming signal. Additionally, we investigate an approach using a combined solar and volcanic forcing variable, with an exponentially decaying response that may be a more realistic temperature response to a change in forcing. Finally, we examine what the residual temperature series looks like if physical climate models are used to remove the effects of volcanoes and solar activity.

2 Multiple linear regression approaches

In order to assess the effectiveness of multiple linear regression approaches, we test two different methods. Specific implementations of these methods can be found in the supplement included along with this manuscript.

2.1 Method 1

$$T_{\mathrm{A}}(t) = \beta_t t + \beta_v V(t - \Delta t_v) + \beta_s S(t - \Delta t_s) + \beta_E E(t - \Delta t_E) \quad (1)$$

ESDD
4, 1065–1090, 2013

In this regression (Eq. 1), the temperature anomaly (T_A) is the dependent variable and time (t), lagged total solar irradiance (solar, S), lagged stratospheric optical thickness (volcanic, V), and lagged Nino3.4 index (ENSO, E) are used as explanatory variables for the temperature evolution. The lag (Δ) for each of the three variables is tested between 0 and 10 months, with every combination attempted, and the best overall combinational fit determined based on the resulting R^2 value of each regression. This leaves a total of seven variables to be computed: 4 coefficients (β_t, β_v, β_s, β_E) and three lags (Δ_v, Δ_s, Δ_E). This mirrors the approach of Foster and Rahmstorf (2011), albeit without the second order Fourier series used to account for residual annual cycles. It is also follows the approach of Lean and Rind (2008), which, although they use a specific variable to represent the anthropogenic forcing rather than a linear time trend, should give nearly the same results over the observed time period when the anthropogenic forcing increase is approximately linear.

2.2 Method 2

The second approach uses multiple linear regressions to fit temperature responses as well, but here we assume that over this time period, the temperature responds to a forcing according to the following simple energy balance model:

$$C\frac{\mathrm{d}T}{\mathrm{d}t} = \Delta F - \lambda \Delta T \tag{2}$$

Where T represents the surface air temperature, C the mixed-layer heat capacity, F the forcing that causes an energy flux into the mixed layer, and λ the strength of radiative restoration. This implies an exponential decaying response to each change in forcing, resulting in the following time-based solution for the temperature anomaly given a single change in forcing:

$$T_A(t) = \lambda^{-1}(\Delta F)(1 - e^{(-\frac{t}{k})}) \tag{3}$$

ESDD
4, 1065–1090, 2013

Here, k represents the e-folding time of the response. In the case of the regression, we can then combine the sunspot observations and stratospheric optical thickness into a single forcing series with units $\mathrm{W\,m^{-2}}$, using approximate physical relationships. The value of 117 (sunspots/TSI) is determined based on the regression of smoothed sunspots against TSI, where TSI is the total solar irradiance in $\mathrm{W\,m^{-2}}$. After accounting for geometry and albedo, this corresponds to approximately 669 sunspots per $\mathrm{Wm^{-2}}$ change in actual solar forcing. For the volcanic forcing, the observed stratospheric aerosol optical depth is converted using the "effective forcing" relationship of $-23\,\mathrm{W\,m^{-2}}\,\tau^{-1}$ based on the GISS Model E calculation.

The linear time trend and ENSO variable remain the same as Method 1, yielding the following regression in this approach:

$$T_{\mathrm{A}}(t) = \beta_t t + \beta_F[F \cdot g(k)](t) + \beta_E V(t - \Delta t_E) \tag{4}$$

F represents the combined solar and volcanic forcing for each month, which is then convolved with the normalized exponential function of e-folding time k, $g(k)$. In this case, just as the various lags (Δ) are tested, so too is the e-folding time (k) varied, and the best resulting match (for all combinations) is determined based on R^2 values. A total of five variables is thus computed: three coefficients (β_t, β_F, β_E), one lag (Δ_E), and one value for the e-folding time (k). The potential advantages of this approach relative to method 1 are two-fold: first, it reduces the number of values to be fitted and thus reduces the risk of over-fitting, and second, it allows large changes in forcings to produce temperature responses that endure beyond the relatively short lag-times calculated in method 1.

2.3 Multiple regression data

As a proxy for solar activity, we use the monthly mean sunspot number from the Solar Influences Data Analysis Center (SIDC) (http://sidc.oma.be/sunspot-data/) at the Royal Observatory of Belgium, acquired via Climate Explorer (http://climexp.knmi.nl/;

ESDD
4, 1065–1090, 2013

Van Oldenborgh et al., 2009). This set has the advantage of providing a monthly resolution back to (and before) 1955, the start of our energy balance model runs, as discussed in Sect. 3.1. Similarly, as a proxy for volcanic activity, we use the observed monthly mean stratospheric optical depth at 550 nm (Sato et al., 1993) available at the NASA Goddard Institute of Space Studies (GISS) website (http://data.giss.nasa.gov/modelforce/strataer/). Finally, to represent ENSO activity, we use the sea surface temperature (SST) anomalies from the Nino3.4 region (Reynolds et al., 2002), acquired via Climate Explorer as well. We use this index rather the Multivariate ENSO Index due to the ease of calculating the Nino3.4 results in the same manner in global climate models.

3 Testing with an energy balance model

3.1 The model

This model takes the form described in Eq. (2). Apart from the longer-term forcings creating the underlying signal, which is discussed in 3.2, the model is forced by three inter-annual-to-decadal scale influences – solar activity, volcanic eruptions, and ENSO. The change in solar and volcanic forcings are determined in the same manner discussed in Sect. 2.2. For ENSO, we "force" the oceanic portion of the model by using the first-order differences in the monthly Nino3.4 index as the change in flux into the mixed layer, multiplied by a scalar factor to roughly simulate the magnitude of observed ENSO fluctuations. In this way, the resulting model-induced temperature fluctuations have the same form as the Nino3.4 index. Note that the ENSO forcing in this model does not operate at the TOA as the other forcings do, and only affects the TOA imbalance insomuch as the induced temperature fluctuations produce an outgoing radiative response.

To produce the "raw" model output, we run the model with all forcings applicable to the test. However, the advantage of using a simple model like this is that we can run

ESDD
4, 1065–1090, 2013

the model quickly with only one forcing turned on at a time, in order to see exactly what each forcing contributes to the temperature change. This can then be compared against the diagnosed contribution, as determined by each of the multiple regression methods run against the raw model output. The degree to which these correspond thus represents the efficacy of the method.

We run the actual tests starting in 1979 for several reasons. First, for comparison with Foster and Rahmstorf (2011). Second, the one-box model is less likely to remain applicable as the timescales grow longer, as ocean heat transport becomes more of a factor. Finally, the time period prior to 1979 is characterized by a cooling that complicates the study of whether the aforementioned methods could detect a potential deceleration in surface warming. Nonetheless, the model is actually started in 1955 to ensure that we have captured the potential natural influence of previous forcings – volcanic eruptions in particular – on the later part of the temperature record.

In terms of actual parameter values used for Eq. (2) in these tests, we chose three different configurations to examine the how different potential underlying aspects of the Earth system would affect the validity of the linear regression assumptions. For the primary configuration, we selected a value of 2.0 $\mathrm{W\,m^{-2}\,K^{-1}}$ for λ, per Masters (2013), which corresponds to an effective sensitivity of 2 K to a doubling of CO_2, and a C of 113 $\mathrm{W\text{-}month\,m^{-2}\,K^{-1}}$ (corresponding to an effective mixed layer of 70 m of water) to approximately fit the observed rise in temperature over this period. This produces an e-folding time, k, in Eq. (3) of 57 months. For a second configuration (alternate A), values are selected to produce a rapid response, with a value of $\lambda = 4.0\,\mathrm{W\,m^{-2}\,K^{-1}}$ (corresponding to effective sensitivity of 1 K) and $C = 57\,\mathrm{W\text{-}month\,m^{-2}\,K^{-1}}$ (35 m of water), such that the resulting value for k is 14 months. For the final configuration (alternate B), we select values to produce a longer response: $\lambda = 1.0\,\mathrm{W\,m^{-2}\,K^{-1}}$ (effective sensitivity of 4 K) and $C = 194\,\mathrm{W\text{-}month\,m^{-2}\,K^{-1}}$ (120 m of water). This produces an e-folding time of $k = 194$ months. Note that these alternate configurations are at the extreme of potential values for the Earth system on the multi-decadal timescale, such that the response time is likely bounded with these configurations. There are a variety

ESDD
4, 1065–1090, 2013

of ways these parameters could be tuned to the observed temperature over the 1979–2012 period, and it is not required that any of these configurations represents the "true" values of the earth system for the simple use of testing the methods. Rather, the goal is simply to see how well the methods can diagnose the forcing responses that are based on these values. The effect of these values on the efficacy of the methods is discussed further in Sect. 3.3.

3.2 Underlying linear and decelerating signal

The "underlying signal" in these tests refers to the progression of the global surface temperature anomaly if the effects of solar, ENSO, and volcanoes could be perfectly removed. In this sense, the underlying signal may be some combination of anthropogenic forcing effects and natural forcings or variability apart from the aforementioned solar, ENSO, and volcanic influences. All of the tests using the simple one-box model include an underlying linearly increasing radiative forcing, which, based on the parameters for the model, produces an approximate linear warming trend of 0.13 K decade^{-1}.

For the tests with an underlying decelerating signal, an oscillating forcing producing a heat flux into the mixed layer (but not a TOA radiative forcing) is layered on top of the underlying linear trend. In the primary configuration, this forcing produces an oscillation in the temperature anomaly with an amplitude of approximately 0.11 K at a frequency of 60 yr. When combined with the underlying linear trend, this has the effect of producing a peak trend of 0.23 K decade^{-1} from 1979–1990 in the underlying signal, which then decelerates to near standstill (0.01 K decade^{-1}) in the last decade. Alternate configurations A and B approximately match this effect, producing trends of 0.22 K decade^{-1} and 0.25 K decade^{-1} from 1979–1990 and trends of −0.01 K decade^{-1} and 0.04 K decade^{-1} from 2003–2012 respectively.

Note that this is not meant to propose a physical basis for such an oscillation, although Kosaka and Xie (2013) suggest that equatorial Pacific surface cooling could result in a deceleration in recent surface temperature trends similar to the one simulated by this model. Nor do we *assume* such a deceleration exists in the real-world

ESDD
4, 1065–1090, 2013

underlying signal. Rather, this is simply used to produce a deceleration in the simulation in order to determine the effectiveness of the above methods in detecting this type of underlying signal (that is, a "slowdown" or pause).

3.3 Results

Figures 1 and 2 show the results of using the two multiple regression methods to reproduce the underlying signal by removing the effects of solar, volcanic, and ENSO influences from the output of the simple one-box energy balance model under the primary configuration. In both the linear and decelerating signal cases, Method 1 performs poorly, overestimating the post-2000 underlying trend by about 1.6 K century^{-1} (Table 1). This is generally the result of two factors. First, the method (using only an undamped, shifted response to the forcing) is unable to account for any enduring recovery from volcanic eruptions – particularly the Mount Pinatubo eruption – beyond the time when the stratospheric aerosols are dissipated plus whatever lag is fit in the method. However, this only represents the end of the forcing, whereas the time to again reach equilibrium after the large volcanic-induced cooling (i.e. the "recovery") takes many years rather than months. The degree of divergence between the volcanic impact diagnosed by the method and the actual volcanic response depends directly on the e-folding time, k (Fig. 3). Under the primary configuration and the slow-response configuration (alternate B), the divergence between the two is large, leading to a misdiagnosis of trend well into the first decade of the 21st century. For the rapid response configuration (alternate A), Method 1 performs better for the volcanic contribution, as the error in this component does not persist into the 21st century. This indicates that the method may decently approximate the volcanic contribution if the actual Earth system exhibits the extremely low sensitivity and mixed layer heat capacity modeled in this configuration. However, note that the effective sensitivity of even the primary configuration is on the low end of CMIP5 AOGCMs, thus producing a relatively short value for the e-folding time k, and the fact that under that scenario Method 1 still underestimates

ESDD
4, 1065–1090, 2013

the warming contribution of Pinatubo to the post-2000 trend indicates it is likely to do so for most realistic values of the Earth system.

The second factor leading toward the overestimation of the post-2000 trend comes from the solar contribution: as there are only a few solar cycles of this period, Method 1 greatly overestimates their influence, thereby overestimating the cooling impact of the decreasing solar activity in the 21st century. This overestimation of the solar influence appears to be robust across all configurations (Fig. 3).

Method 2 performs extremely well in all aspects of attribution for the linear signal case. This should come as no surprise, as the exponential decay function (Eq. 3) expects a model of exactly the form used to create the test (Eq. 2). This is what makes the second test – a decelerating signal – of interest, whereby the model used to estimate the signal assumes the exactly correct form and magnitude of forcings and ENSO, with only the assumption of a linear underlying trend being incorrect. As Fig. 2. indicates, such a scenario still leads to an underestimation of the warming contribution from Pinatubo. The result is that the post-2000 trend is actually adjusted in the wrong direction (upward) relative to the trend in the raw model output, and the resulting estimate is a trend more than 3 times larger than the true underlying trend in the signal. Clearly, the choice of the assumed underlying signal has a major impact in these types of analysis.

It should be noted that the ENSO influence is not shown in Figs. 1 and 2. This is because the "reconstructed" ENSO impacts match the true ENSO impacts almost perfectly. While much of this may be largely the result of the same form and index is used for the test generation and in the multiple regressions methods, it also suggests that these ENSO variations may be of high enough frequency for their estimate to be insensitive to the assumed underlying signal in the tests.

ESDD
4, 1065–1090, 2013

4 Testing with CMIP5 models

4.1 Method

For a second set of tests, we use more comprehensive global climate models from the Coupled Model Intercomparison Project phase 5 (CMIP5) as a check on the efficacy of the methods under arguably more realistic scenarios. Using the CMIP5 historical/RCP scenario simulations is problematic, as it would require some means of decomposing those runs into their various contributions (anthropogenic, solar, volcanic, ENSO), which is the very type of method we are attempting to validate. However, by using the natural-forcing-only runs, we can find an estimate of the combined solar and volcanic influence, and simply add the same underlying decelerating signal from Sect. 3.2 on top of this natural variation.

The forced response from solar plus volcanic activity is assumed to be the mean of the natural-only runs for a particular model. To have higher confidence that we have captured only the forced response, only models with a large number of runs are used in these tests – in this case, GISS-E2-R (10 runs) and CNRM-CM5 (6 runs). Furthermore, these are among the better models at simulating ENSO processes (Bellenger et al., 2013). For estimating the ENSO influence, the high-frequency "unforced" variation in these model runs – calculated by subtracting the mean of the ensemble from the individual run – is assumed to arise primarily from these ENSO processes.

4.2 Data

The climate model runs come from the CMIP5 natural-forcing-only ensemble. This series of runs was acquired from the ETHZ CMIP5 sub-archive and average anomalies were calculated for surface-air temperature (tas) globally, and for the Nino3.4 region (5° N to 5° S, 170° W to 120° W). The models shown in Fig. 4, and included in the Sect. 5 adjustments, were chosen based on those having 4 or more runs of the natural-only

ESDD
4, 1065–1090, 2013

experiment available in this CMIP5 sub-archive: GISS-E2-R, GISS-E2-H, CanESM2, CNRM-CM5, CSIRO-Mk3.6.0, CCSM4, HadGEM2-ES.

4.3 Results

Both methods 1 and 2 generally perform on par with one another when tested on global climate models with underlying decelerating signals (Figs. 5 and 6). Again, both of these methods do poorly in reconstructing the true underlying signal, largely because of the volcanic influence. However, the large positive ENSO influence to post-2000 temperatures in the CNRM-CM5 run ($1.3\,\mathrm{K\,century^{-1}}$) examined is estimated to be a negative influence ($-0.2\,\mathrm{K\,century^{-1}}$) by both methods, which also contributes to the overestimation of the underlying signal. This may suggest that as the proxy for ENSO (the Nino3.4 SST in this case) diverges from the actual influence of ENSO, the diagnosis of this component becomes more sensitive to the accuracy of other forms of the method's model.

The results for tests using the CMIP5 runs on the 21st century trends can be seen in Table 1. The inability of either of the methods to correctly identify the near-pause in the post-2000 simulations indicates that including a linear time regression in the statistical model will give largely misleading results when the underlying signal deviates from this linearity, particularly when coinciding with the recovery from Pinatubo. Despite the methods seemingly removing the uncertainty in the Ordinary Least Squares trends of their adjusted series relative to the trend of the unadjusted series, this tends to result from the attenuation of the higher frequency variations, whereas the lower frequency signal or trend is in fact barely more accurate than in the unadjusted series (and commonly experiences a degradation in accuracy).

ESDD
4, 1065–1090, 2013

5 New adjusted series

5.1 Method

As an alternative to the simple multiple regressions methods described above, we propose removing solar and volcanic influences from the observed record using physical models. In this case, the multi-model mean of the CMIP5 natural-only forcing ensemble provides an estimate of the potential contribution of those elements to the temperature evolution. Thus, in our method, we first subtract the multi-model mean of the natural-only forcings from the observed temperature record.

Since the effects of ENSO begin to average out across all natural-only forcing model runs, an additional step is required to remove ENSO for the observed temperature record, which is done via a regression to determine the lag and effect of ENSO, similar to the other methods. However, the higher-frequency ENSO fluctuations are little affected by the form of the underlying trend in the regression, while the lower-frequency variations (solar and volcanic) that would be sensitive to such forms have already been removed based on physical modeling. This, combined with the fewer parameters in the regression (thereby reducing the risk of over-fitting), is why the ENSO-only regression is likely to avoid the pitfalls of the combined ENSO-solar-volcanic multiple linear regressions.

Given evidence of over-sensitivity to radiative forcings during this time period in the CMIP5 models (Masters, 2013), we suggest the multi-model natural-forcing-only mean likely represents an upper bound of the volcanic and solar influence. We also present an analysis where the impact of volcanic and solar radiative forcings is assumed to be only 50 % of the impact as determined by this modelled mean. Due to the transient nature of these particular influences, and the knowledge that the difference in the transient climate response (TCR) is less than the potential difference in the equilibrium climate sensitivity (ECS), we suggest this is a reasonable lower-bound for solar and volcanic contributions.

ESDD
4, 1065–1090, 2013

It should be noted that while the 50 % adjustment above can be made to account for the difference in the potential magnitude of the solar and volcanic influences in the actual Earth system vs. the CMIP5 multi-model-mean, this does not necessarily take into account the difference in *timing* of the responses. Thus, this method relies to some degree on the multi-model-mean approximately matching the actual response time of the real world.

5.2 Data

For the primary analysis of the actual temperature record, we use the combined land-surface air and sea-surface water temperature anomalies from GISTEMP (Hansen et al., 2010). Additionally, we consider temperature anomalies from HadCRUT4 (Jones et al., 2012), in order to ensure there is not a strong sensitivity to this choice.

5.3 Results

The results of the two potential GISTEMP adjusted series to find the underlying signal can be seen in Fig. 7. In both the full multi-model-mean and the 50 % multi-model-mean adjusted cases for these new temperature reconstructions, a significant (99 %) quadratic term is found when using ordinary least squares, with the Akaike information criterion (AIC) indicating the quadratic as a better model than the simple linear. However, it should be noted that the magnitude of the deceleration varies between the two, with the full multi-model-mean adjustment indicating a deceleration of $-0.110 \pm 0.014\,\mathrm{K\,dec^{-2}}$ vs. the 50 % multi-model mean suggesting a magnitude of $-0.055 \pm 0.013\,\mathrm{K\,dec^{-2}}$. The same is true when using HadCRUTv4 instead of GISTEMP for the temperature series, yielding magnitudes of $-0.066 \pm 0.012\,\mathrm{K\,dec^{-2}}$ and $-0.121 \pm 0.013\,\mathrm{K\,dec^{-2}}$. The calculated magnitude of the ENSO term is relatively insensitive to the underlying form of the time regression (linear vs. quadratic), with the coefficient only differing by a maximum of 12 %, which occurs in the 50 % multi-model-mean adjustment of GISTEMP case.

ESDD
4, 1065–1090, 2013

6 Discussion and conclusions

In general, we found that using multiple linear regressions for attribution of ENSO, volcanic, and solar influences during this time period tends to misdiagnose the underlying surface temperature warming, particularly in the situation where the underlying warming is not strictly linear. The degree to which this method misdiagnoses the recent warming trend largely depends on the magnitude and duration of the Pinatubo recovery. While approaches using linear regressions (Lean and Rind, 2008; Foster and Rahmstorf, 2011) tend to diagnose small volcanic recoveries, more physical models (Merlis et al., 2013; Rypdal, 2012) suggest a longer recovery. The sensitivity to the form of the underlying warming highlights the danger of multiple linear regressions when other important factors may be missing (Benestad and Schmidt, 2009). Moreover, this result generally agrees with other recent papers that the observed pause is unlikely to have resulted from contributions of the solar minimum or volcanic aerosols to the TOA forcing (Guemas et al., 2013; Watanabe et al., 2013), suggesting some other decadal variability is acting upon the surface temperature record. This raises the question of what such variability may have contributed to the warming in prior decades.

Our attempts to estimate the volcanic and solar contributions to the surface temperature evolution using multiple climate models leaves a residual warming signal with a significant deceleration. Again, the extent of the actual deceleration depends on what the Pinatubo recovery has contributed. Furthermore, if the pause in this underlying warming is indeed the result of more efficient ocean heat uptake or some short-lived natural variability, a continuation of the deceleration is unlikely given the observed positive downward TOA imbalance (Loeb et al., 2012).

Supplementary material related to this article is available online at http://www.earth-syst-dynam-discuss.net/4/1065/2013/esdd-4-1065-2013-supplement.zip.

ESDD
4, 1065–1090, 2013

Acknowledgements. I would like to thank Kevin Cowtan of the University of York for helpful comments and discussion in the preparation of this manuscript, and Urs Beyerle for his assistance in accessing the ETHZ CMIP5 sub-archive.

References

Bellenger, H., Guilyardi, E., Leloup, J., Lengaigne, M., and Vialard, J.: ENSO representation in climate models: from CMIP3 to CMIP5, Clim. Dynam., in press, doi:10.1007/s00382-013-1783-z, 2013.

Benestad, R. E. and Schmidt, G. A.: Solar trends and global warming, J. Geophys. Res.-Atmos., 14, D14101, doi:10.1029/2008JD011639, 2009.

Foster, G. and Rahmstorf, S.: Global temperature evolution 1979–2010, Environ. Res. Lett., 6, 044022, doi:10.1088/1748-9326/6/4/044022, 2011.

Guemas, V., Doblas-Reyes, F. J., Andreu-Burillo, I., and Asif, M.: Retrospective prediction of the global warming slowdown in the past decade, Nature Climate Change, 3, 649–653, doi:10.1038/nclimate1863, 2013.

Hansen, J., Ruedy, R., Sato, M., and Lo, K.: Global surface temperature change, Rev. Geophys., 48, RG4004, doi:10.1029/2010RG000345, 2010.

Jones, P. D., Lister, D. H., Osborn, T. J., Harpham, C., Salmon, M., and Morice, C. P.: Hemispheric and large-scale land-surface air temperature variations: an extensive revision and an update to 2010, J. Geophys. Res., 117, D05127, doi:10.1029/2011JD017139, 2012.

Kaufmann, R. K., Kauppi, H., Mann, M. L., and Stock, J. H.: Reconciling anthropogenic climate change with observed temperature 1998–2008, P. Natl. Acad. Sci. USA, 108, 11790–11793, doi:10.1073/pnas.1102467108, 2011.

Keenlyside, N. S., Latif, M., Jungclaus, J., Kornblueh, L., and Roeckner, E.: Advancing decadal-scale climate prediction in the North Atlantic sector, Nature, 453, 84–88, doi:10.1038/nature06921, 2008.

Kosaka, Y. and Xie, S. P.: Recent global-warming hiatus tied to equatorial Pacific surface cooling, Nature, 501, 403–407, doi:10.1038/nature12534, 2013.

Lean, J. L. and Rind, D. H.: How natural and anthropogenic influences alter global and regional surface temperatures: 1889 to 2006, Geophys. Res. Lett., 35, L18701, doi:10.1029/2008GL034864, 2008.

ESDD

4, 1065–1090, 2013

Loeb, N. G., Lyman, J. M., Johnson, G. C., Allan, R. P., Doelling, D. R., Wong, T., Soden, B. J., and Stephens, G. L.: Observed changes in top-of-the-atmosphere radiation and upper-ocean heating consistent within uncertainty, Nat. Geosci., 5, 110–113, doi:10.1038/ngeo1375, 2012.

Masters, T.: Observational estimate of climate sensitivity from changes in the rate of ocean heat uptake and comparison to CMIP5 models, Clim. Dynam., in press, doi:10.1007/s00382-013-1770-4, 2013.

Merlis, T. M., Held, I. M., Stenchikov, G. L., and Zeng, F.: Constraining transient climate sensitivity using coupled climate model simulations of volcanic eruptions, J. Climate, submitted, 2013.

Mochizuki, T., Ishii, M., Kimoto, M., Chikamoto, Y., Watanabe, M., Nozawa, T., Sakamoto, T. T., Shiogama, H., Awaji, T., Sugiura, N., Toyoda, T., Yasunaka, S., Tatebe, H., and Mori, M.: Pacific decadal oscillation hindcasts relevant to near-term climate prediction, P. Natl. Acad. Sci. USA, 1833–1837, doi:10.1073/pnas.0906531107, 2010.

Neely III, R. R., Toon, O. B., Solomon, S., Vernier, J. P., Alvarez, C., English, J. M., Rosenlof, K. H., Mills, M. J., Bardeen, C. G., Daniel, J. S., and Thayer, J. P.: Recent anthropogenic increases in SO_2 from Asia have minimal impact on stratospheric aerosol, Geophys. Res. Lett., 40, 999–1004, doi:10.1002/grl.50263, 2013.

Reynolds, R. W., Rayner, N. A., Smith, T. M., Stokes, D. C., and Wang, W.: An improved in situ and satellite SST analysis for climate, J. Climate, 15, 1609–1625, doi:10.1175/1520-0442(2002)015<1609:AIISAS>2.0.CO;2, 2002.

Rypdal, K.: Global temperature response to radiative forcing: solar cycle vs. volcanic eruptions, J. Geophys. Res.-Atmos, 117, D06115, doi:10.1029/2011JD017283, 2012.

Sato, M., Hansen, J. E., McCormick, M. P., and Pollack, J. B.: Stratospheric aerosol optical depths, 1850–1990, J. Geophys. Res.-Atmos, 98, 22987–22994, doi:10.1029/93JD02553, 1993.

Solomon, S., Rosenlof, K. H., Portmann, R. W., Daniel, J. S., Davis, S. M., Sanford, T. J., and Plattner, G. K.: Contributions of stratospheric water vapor to decadal changes in the rate of global warming, Science, 327, 1219–122, doi:10.1126/science.1182488, 2010.

van Oldenborgh, G. J., Drijfhout, S., van Ulden, A., Haarsma, R., Sterl, A., Severijns, C., Hazeleger, W., and Dijkstra, H.: Western Europe is warming much faster than expected, Clim. Past, 5, 1–12, doi:10.5194/cp-5-1-2009, 2009.

ESDD
4, 1065–1090, 2013

Watanabe, M., Kamae, Y., Yoshimori, M., Oka, A., Sato, M., Ishii, M., and Kimoto, M.: Strengthening of ocean heat uptake efficiency associated with the recent climate hiatus, Geophys. Res. Lett., 40, 3175–3179, doi:10.1002/grl.50541, 2013.

ESDD
4, 1065–1090, 2013

Table 1. Ordinary Least Squares (OLS) trends calculated from "raw" and "adjusted" series from simulated 2000–2012 using tests described in Sects. 3 and 4, along with 95 % confidence intervals. Method 1 and Method 2 trends represent the attempts to find the underlying trend using those respective methods.

	Raw Trend (K century^{-1})	Meth 1 Trend (K century^{-1})	Meth 2 Trend (K century^{-1})	Underlying Trend (K century^{-1})
1-Box Linear (Primary)	1.68 ± 0.39	2.91 ± 0.12	1.24 ± 0.05	1.32
1-Box Decel (Primary)	0.57 ± 0.39	1.84 ± 0.13	0.76 ± 0.04	0.21
1-Box Linear (Alt. A)	0.54 ± 0.30	1.45 ± 0.11	1.18 ± 0.14	1.32
1-Box Decel (Alt. A)	−0.55 +/0.30	0.43 ± 0.11	0.07 ± 0.14	0.23
1-Box Linear (Alt. B)	2.55 ± 0.33	3.26 ± 0.08	1.57 ± 0.03	1.34
1-Box Decel (Alt. B)	1.73 ± 0.35	2.55 ± 0.11	1.36 ± 0.02	0.53
GISS-E2-R	1.18 ± 0.50	1.08 ± 0.46	0.98 ± 0.46	0.21
CNRM-CM5	2.07 ± 0.71	2.60 ± 0.48	2.45 ± 0.48	0.21

ESDD
4, 1065–1090, 2013

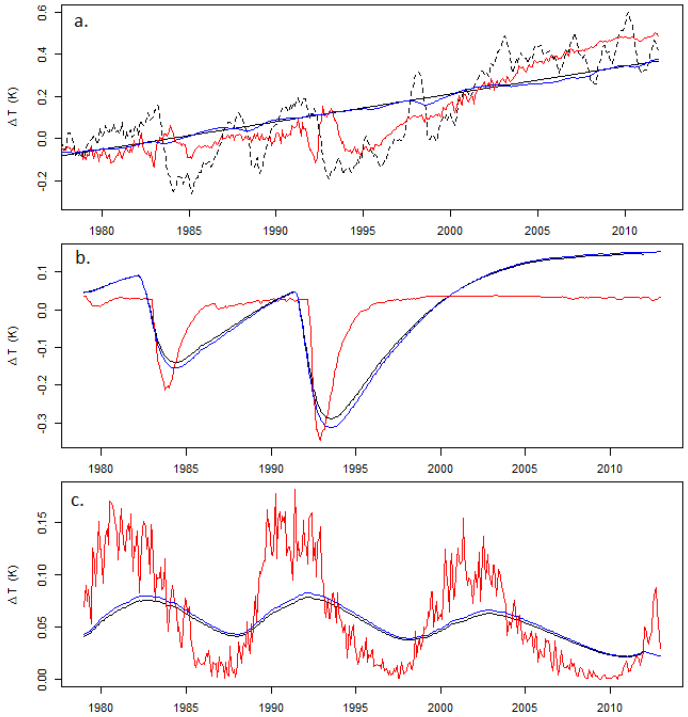

Fig. 1. Primary configuration of one-box energy balance model with underlying linear trend. **(a)** Output from simple energy balance model using volcanic, solar, and ENSO influences on top of an underlying linear trend (dashed-black), the underlying trend only (solid black), the adjusted temperatures using Method 1 (red), and the adjusted temperatures using Method 2 (blue). **(b)** Volcanic contribution. The energy-balance model run with only volcanic contribution (black), the diagnosed volcanic contribution using Method 1 (red), and the diagnosed volcanic contribution using Method 2 (blue). **(c)** Solar contribution. The energy-balance model run with only solar contribution (black), the diagnosed solar contribution using Method 1 (red), and the diagnosed solar contribution using Method 2 (blue).

ESDD
4, 1065–1090, 2013

Problems with solar, volcanic, and ENSO attribution

T. Masters

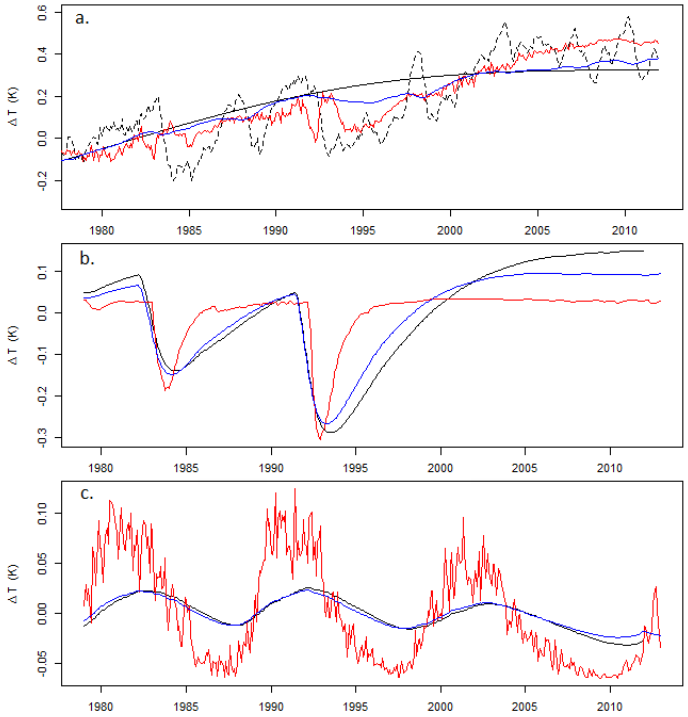

Fig. 2. Primary configuration of one-box energy balance model with deceleration of underlying surface warming signal. **(a)** Output from simple energy balance model using volcanic, solar, and ENSO influences on top of an underlying decelerating signal (dashed-black), the underlying signal only (solid black), the adjusted temperatures using Method 1 (red), and adjusted temperatures using Method 2 (blue). **(b)** Volcanic contribution. The energy-balance model run with only volcanic contribution (black), the diagnosed volcanic contribution using Method 1 (red), and the diagnosed volcanic contribution using Method 2 (blue). **(c)** Solar contribution. The energy-balance model run with only solar contribution (black), the diagnosed solar contribution using Method 1 (red), and the diagnosed solar contribution using Method 2 (blue).

ESDD
4, 1065–1090, 2013

Problems with solar, volcanic, and ENSO attribution

T. Masters

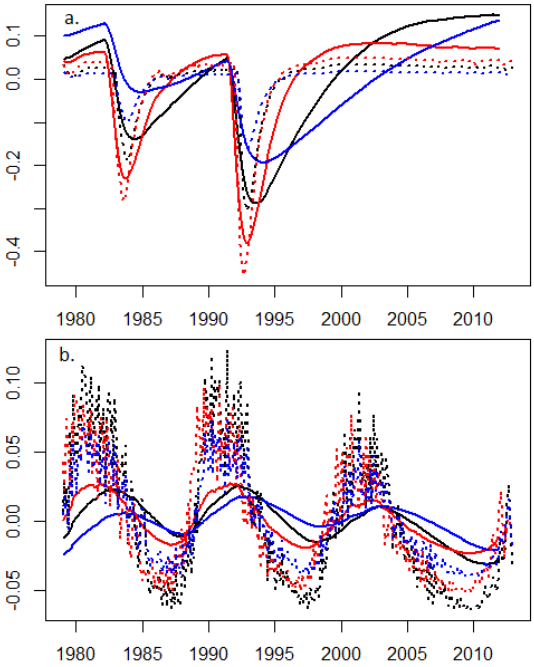

Fig. 3. Different configurations of one-box energy balance model with deceleration of underlying surface warming signal. **(a)** Volcanic contribution. The actual energy-balance model runs with only volcanic contribution (solid) vs. the diagnosed volcanic contribution using Method 1 (dashed) for $k = 55$ months (black), $k = 14$ months (red), and $k = 194$ months (blue). **(b)** Solar contribution. The actual energy-balance model runs with only solar contribution (solid) vs. the diagnosed solar contribution using Method 1 (dashed).

ESDD
4, 1065–1090, 2013

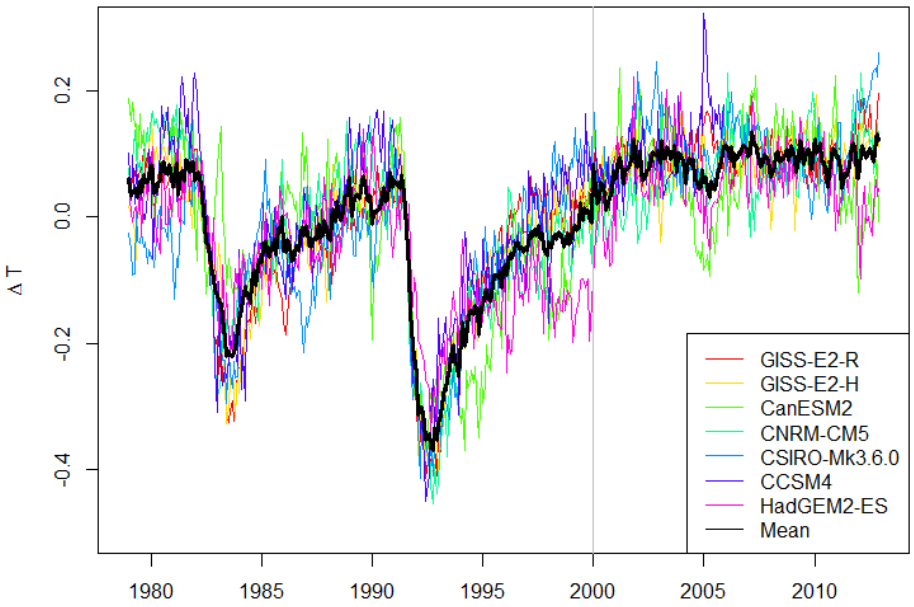

Fig. 4. Mean of the CMIP5 Natural Forcing Only ensembles for models with 4 or more runs. The black line represents the mean of these models with the exception of CCSM4, which does not run all the way to 2012.

ESDD
4, 1065–1090, 2013

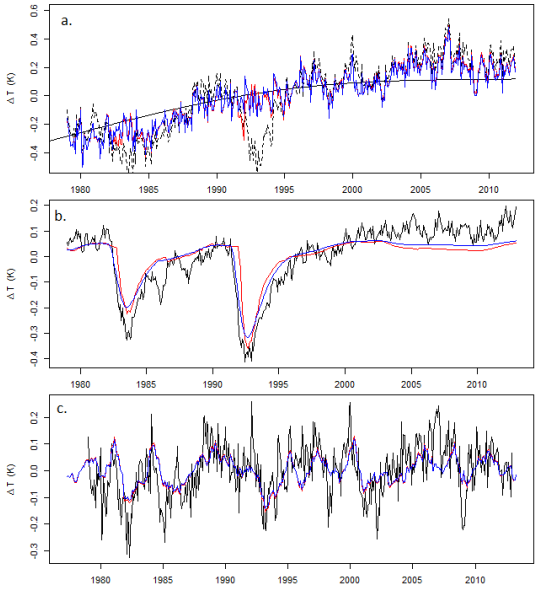

Fig. 5. GISS-E2-R. **(a)** Natural-only forcing run 1 with added signal of decelerating surface warming (dashed-black), this underlying signal only (solid black), the adjusted temperatures using Method 1 (red), and the adjusted temperatures using Method 2 (blue). **(b)** Volcanic and solar contributions. The mean of 10 GISS-E2-R natural-only forcing runs representing the combined volanic and solar contribution (black), the diagnosed volcanic plus solar contribution using Method 1 (red), and the diagnosed volcanic plus solar contribution using Method 2 (blue). **(c)** ENSO contribution. The difference between the single GISS-E2-R run and the mean of 10 GISS-E2-R natural-forcing-only runs representing the ENSO contribution (black), the diagnosed ENSO contribution using Method 1 (red), and the diagnosed ENSO contribution using Method 2 (blue).

ESDD
4, 1065–1090, 2013

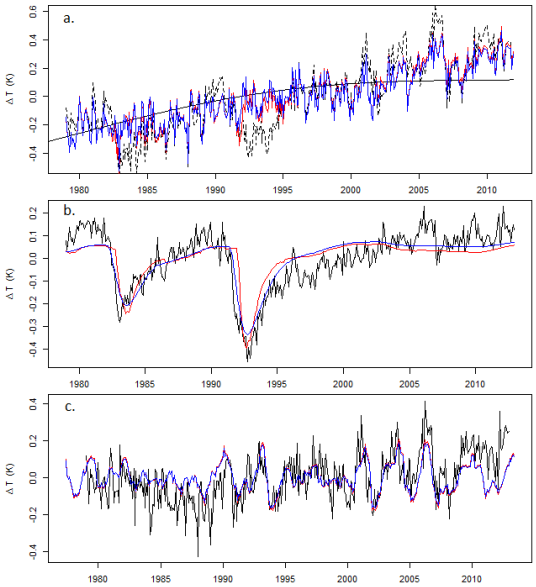

Fig. 6. CNRM-CM5. **(a)** Natural-only forcing run 1 with added signal of decelerating surface warming (dashed-black), this underlying signal only (solid black), the adjusted temperatures using Method 1 (red), and the adjusted temperatures using Method 2 (blue). **(b)** Volcanic and solar contributions. The mean of 6 CNRM-CM5 natural-only forcing runs representing the combined volanic and solar contribution (black), the diagnosed volcanic plus solar contribution using Method 1 (red), and the diagnosed volcanic plus solar contribution using Method 2 (blue). **(c)** ENSO contribution. The difference between the single CNRM-CM5 run and the mean of 6 CNRM-CM5 natural-forcing-only runs representing the ENSO contribution (black), the diagnosed ENSO contribution using Method 1 (red), and the diagnosed ENSO contribution using Method 2 (blue).

ESDD
4, 1065–1090, 2013

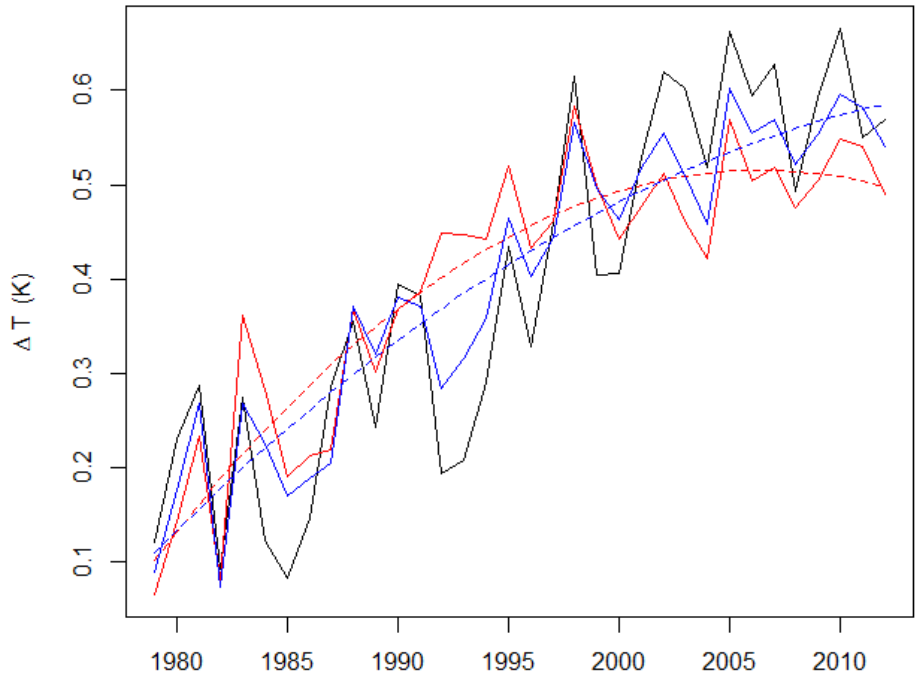

Fig. 7. Unadjusted annual average of GISTEMP (black), annual average of GISTEMP adjusted by the full natural-only multi-model mean with ENSO effects removed (solid red) and its quadratic fit (dashed red), as well as the annual average of GISTEMP adjusted by 50 % times the natural-only multi-model mean with ENSO effects removed (solid blue) and its quadratic fit (dashed blue).

ESDD
4, 1065–1090, 2013